Pharm Res (2015) 32:702–713
DOI 10.1007/s11095-014-1498-9

RESEARCH PAPER

# Simultaneous Formation and Micronization of Pharmaceutical Cocrystals by Rapid Expansion of Supercritical Solutions (RESS)

Katrin C. Müllers • Maria Paisana • Martin A. Wahl

Received: 4 June 2014 / Accepted: 20 August 2014 / Published online: 12 September 2014


## ABSTRACT

***Purpose*** We investigated the RESS process as a means of simultaneous micronization and cocrystallization of a model drug with poor aqueous solubility.

***Methods*** 1:1 cocrystals of ibuprofen (IBU) and nicotinamide (NA) were produced with a pilot scale unit for RESS processing.IBU and NA were dissolved in $scCO_2$ at 30 MPa and 50°C. After 24 h, the supercritical solution was expanded at a medium $CO_2$ flow rate of 3.8 kg/h during 60 min into an expansion vessel kept at ambient conditions. Cocrystals were identified with DSC, XRD and confocal Raman microscopy (CRM) and further characterized by SEM, specific surface area, wetting ability, solubility and dissolution testing.

***Results*** Judging by DSC, XRD and CRM, cocrystals with high purity could be produced with the RESS technique. Micronization *via* RESS was successful, since the specific surface area of RESS cocrystals was increased almost tenfold in comparison to cocrystals produced by slow solvent evaporation. Due to the additional micronization, the mean dissolution time of IBU from RESS cocrystals was decreased.

***Conclusions*** RESS cocrystallization offers the advantage of combining micronization and cocrystallization in a single production step. For drugs with dissolution-limited bioavailability, RESS cocrystallization may therefore be a superior approach in comparison to established cocrystallization techniques.

**KEY WORDS** cocrystals · dissolution · ibuprofen · RESS · supercritical fluids

K. C. Müllers • M. A. Wahl (✉)
Institut für Pharmazeutische Technologie
und Biopharmazie, Pharmazeutisches Institut, Eberhard Karls Universität
Tübingen, Auf der Morgenstelle 8, 72076 Tübingen, Germany
e-mail: Martin.Wahl@uni-tuebingen.de

M. Paisana
Departamento de Farmácia Galénica e Tecnologia
Farmacêutica, Faculdade de Farmácia, Universidade
de Lisboa, Av. Prof. Gama Pinto, 1649-003 Lisbon, Portugal

## ABBREVIATIONS

| | |
|---|---|
| IBU | Ibuprofen |
| NA | Nicotinamide |
| RCC 0.5:1 | RESS coprecipitates with a molar ratio of 0.5:1 (IBU:NA) |
| RCC 1:1 | RESS coprecipitates with a molar ratio of 1:1 (IBU:NA) |
| SCC 1:1 | Cocrystals produced by slow solvent evaporation |
| $ScCO_2$ | Supercritical carbon dioxide |

## INTRODUCTION

Cocrystallization is a useful way of improving the physicochemical properties of pharmaceuticals; especially, if the respective drug is non-ionisable and thus salt formation is not possible [1]. In cocrystals, a pharmaceutically active ingredient (API) and a structurally related additive are distributed homogeneously in a definite stoichiometric ratio and engage on a supramolecular level *via* non-ionic interactions [1, 2]. Cocrystals are most commonly prepared by slow evaporation of organic solvent, or slow cooling from a solution of the cocrystal formers in organic solvent. These production methods, however, bear the risk of crystallizing the single component phases and thus obtaining a product with phase impurities [3, 4]. In that case, experimental conditions need to be determined empirically, which often involves a lot of laboratory work, or knowledge of the ternary phase diagrams of cocrystal formers and the respective solvent is required [3]. In addition, remaining residues of the solvents may contaminate the product. A production method that avoids this and invariably leads to the formation of cocrystals would therefore be desirable. In this context, Rapid Expansion of Supercritical Solutions (RESS) might provide crystallization conditions that suppress the segregation of the single components and lead to the formation of a pure cocrystal product. During RESS, a

solution of one or more solids in, most commonly, supercritical carbon dioxide ($scCO_2$) is rapidly depressurized to atmospheric conditions [5]. The expansion period occurs in less than $10^{-5}$ s; therefore, the solvent power of the fluid, which is a direct function of the supercritical fluid density, drops dramatically and results in high supersaturation S of the solute in the depressurized fluid [5, 6]. S is defined as

$$S = \frac{\gamma_E(p_E; T_E)}{\gamma^*(p; T)} \quad (1)$$

Where $\gamma_E$ is the solute mole fraction at the extraction temperature and pressure ($T_E$; $p_E$) and $\gamma^*$ is the equilibrium mole fraction of the solute at the actual temperature and pressure of expansion (p;T) [5]. The supersaturation is the driving force that leads to nucleation and crystallization, which results in the precipitation of fine particles in the micron and submicron or even nano range [7, 8]. The RESS process is an attractive micronization technique, since it is based on the use of a non-toxic, highly volatile solvent instead of toxic organic solvents [9]. If, as suggested in this work, cocrystallization is combined with RESS, contamination of the final product with solvent residues can thus be avoided as opposed to cocrystallization from organic solvents [10]. With RESS, no organic solvent waste is generated, which is in fact a major issue from both an economic and an environmental standpoint, since organic solvents typically account for 80–90% of the mass balance of a pharmaceutical batch operation [11]. Compared to spray-drying or milling, neither high temperatures nor mechanical stress are imposed in RESS, which could cause chemical and thermal degradation or the formation of partially or completely amorphous products [12]. A disadvantage of the RESS process is the often limited solubility of pharmaceutical compounds in the respective fluids [13]. This, however, can be overcome by a continuously running process, especially if the low cost of carbon dioxide and the option of in-system recycling of the fluid are considered. Low product yields may also be caused by inefficient separation from the expansion jet and collection of particles [14] or potential blockage of the nozzle due to Joule-Thompson cooling caused by the expansion of the fluid [12]. These problems can, however, be reduced by well defined working conditions.

In the pharmaceutical field, the RESS process has been mostly used for particle design and micronization [6–8, 15–17]. However, the possibility of precipitating an API together with an excipient and thus forming functionalized and micronized drug particles in a single production step makes the RESS process a highly interesting tool. Vemavarapu *et al.* first assessed RESS as a technique for crystal doping and coprecipitation of a large number of pharmaceuticals, and found that depending on the solubility and affinity of the components towards the supercritical solvent, cocrystal formation could be observed among other phenomena such as hydrate formation or polymorphic transition [18]. The authors however found that supercritical solvent assisted cocrystallization was limited due to the fact that selective extraction of the components leads to inhomogeneous mixtures and thus incorrect stoichiometry of the supercritical solution. Selective extraction occurs, when one of the components presents a much larger solubility in $scCO_2$ than the other, which was reported for theophylline (THEO) and caffeine (CAF) [18]. CAF was found to exceed the solubility of THEO by one order of magnitude in previous studies, which will lead to a supercritical solution with according stoichiometry if the solids are presented in a 1:1 ratio [19]. In a different study, cocrystallization of indomethacin (IND) and saccharin (SAC) was attempted *via* a supercritical solvent technique, which proved unsuccessful, since the solubility in $scCO_2$ of both the pure components was too low [20]. In the present study, we therefore focused on precipitating a cocrystal structure from a supercritical solvent with components that both have sufficient solubility in $scCO_2$. We furthermore present a more comprehensive pharmaceutical characterization of the cocrystals we produced with RESS, with particular regard to the product purity. The model API under investigation in this work is ibuprofen (IBU) since its high solubility in $scCO_2$ makes it a good candidate for precipitation in the RESS process [6, 21]. IBU classifies as a Class II drug according to the Biopharmaceutics Classification System due to its low dissolution rate and aqueous solubility. A 1:1 cocrystal structure of IBU and nicotinamide (NA) obtained by solvent evaporation, grinding and hot melt extrusion has been previously described and shown to have a higher intrinsic dissolution rate of IBU compared to the pure drug [4, 22–25]. The cocrystal assembly consists of a central NA amide dimer and linkages to carboxylic acid functions of IBU *via* the pyridine ring of NA (Fig. 1) [23]. Even though both NA and IBU present sufficiently high solubility in $scCO_2$ [21, 26], the difference in solubility between the compounds is at least one order of magnitude, which needs to be considered in order to obtain a supercritical solution with the correct stoichiometry for cocrystal formation. As stated above, the RESS process offers the advantage of simultaneous product micronization, which is of particular interest for poorly soluble drugs with dissolution-limited bioavailability such as IBU. This study therefore focuses on the identification of the process conditions necessary for the production of a pure cocrystalline phase with the RESS process. In addition, the impact of the production technique on the particle morphology and dissolution performance of the API and its cocrystal with NA was studied.

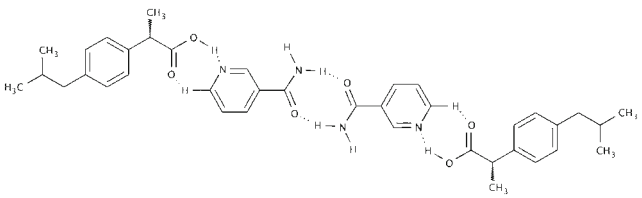

**Fig. 1** Molecular assembly of the 1:1 R,S-IBU NA cocrystal [23].

## MATERIALS AND METHODS

### Materials

Micronized R,S-ibuprofen (IBU) with a median particle size (Dv50) of 50 µm was purchased from BASF (Ludwigshafen, Germany). Nicotinamide (NA) was purchased from Caelo (Bonn, Germany). Carbon dioxide ($CO_2$) was purchased from Air Liquide (Düsseldorf, Germany). All other chemicals were obtained in the purest grade available from Merck (Darmstadt, Germany).

### Production of RESS IBU and Cocrystals with the RESS Process

A pilot unit for supercritical fluid extraction (Sitec-Sieber, Maur, Switzerland) was modified for high-pressure micronization and coprecipitation (Fig. 2). The materials were placed inside the extraction chamber with a volume of 5 l, which was subsequently flooded with $CO_2$ at a temperature of 50°C and a pressure of 30.0 MPa. These extraction conditions were chosen in order to achieve maximum NA solubility in $scCO_2$ [26]. Prior to expansion, the solution was left to reach equilibrium. In the case of RESS IBU, the amount of solid in the extraction chamber was 2.0 g and the equilibration time was 3 h. For the production of cocrystals, an accurately weighed amount of IBU (see below) and an excess of solid NA were placed in the extraction chamber and left to equilibrate over 24 h.

After the appropriate time of extraction, the supercritical solutions were expanded during 1 h through a 150 µm nozzle into the expansion chamber at a medium flow rate of 3.8 kg/h. To compensate for the cooling effect of expanding $scCO_2$ inside the expansion chamber, the temperature control of the mantle was set to 50°C. Temperature and pressure inside the extraction and expansion chambers were monitored during the expansion process (VisiDAQ Runtime software version 3.11). The particles were precipitated onto a filter and the gaseous $CO_2$ was removed from the expansion chamber by a suction pump attached to the outlet to maintain ambient pressure. Prior to particle collection, the expansion chamber was allowed to equilibrate in order to prevent potential condensation of air moisture on the products.

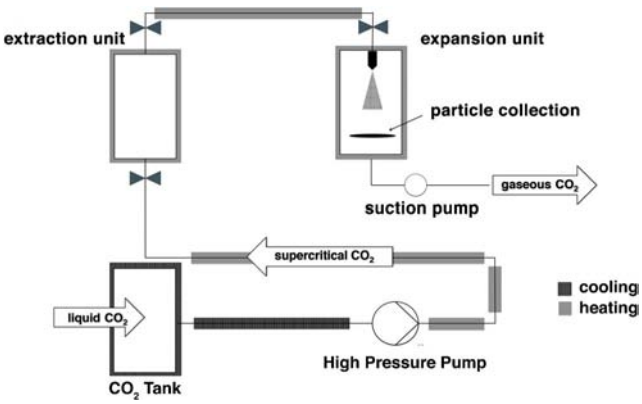


**Fig. 2** Schematic of the pilot unit for RESS processing.

#### *Solubility in $scCO_2$*

IBU was freely soluble in $scCO_2$ at the given experimental conditions. The solubility of NA in $scCO_2$ was determined gravimetrically after the end of the experiment by accurately weighing the undissolved remnant inside the extraction chamber. The solubility was calculated as molar fraction of $scCO_2$ inside the extraction chamber. At 30.0 MPa and 50°C, the static solubility of NA was found to be $y = 5.55 \times 10^{-5}$ mol fraction ($n = 8$). At this point, 61.5 ± 5.8% of the original amount (1.0 g) were dissolved. For the production of coprecipitates with different molar ratios of the 2 compounds, the equilibrium solubility of NA was exploited while the mass of solid IBU was varied accordingly in the extraction chamber to achieve the desired mole fractions in solution; *i.e.* 0.5:1; 1:1 or 2:1 molar ratio (IBU:NA) in $scCO_2$. The quantitative composition of the coprecipitated RESS products was verified by HPLC (see below).

### Preparation of IBU NA Cocrystals by Slow Solvent Evaporation

Cocrystals of IBU and NA in a molar ratio of 1:1 were prepared by slow solvent evaporation as a reference production method for cocrystals. Equimolar solutions of IBU and NA were prepared in ethanol (purity 96%) and then joined in equal volumes into petri dishes. The solvent was left to evaporate slowly at ambient conditions during 24 h. The petri dishes were then placed into an oven at 30°C for 6 h to remove the remaining solvent. Subsequently, the samples were triturated gently with a pestle and mortar and passed through a 250 µm sieve to obtain a fraction with a similar BET surface area to the unprocessed material for dissolution studies (see below).

### Identification and Characterization of Cocrystals

#### *Differential Scanning Calorimetry (DSC)*

Measurements were performed using a DSC system (TA 8000, DSC 820, Mettler Toledo, Germany). The samples (4.5–5.5 mg per run) were placed in perforated 40 µl aluminium standard pans and crimped with punched lids. An empty aluminium sample pan was used as reference. The heating rate was set to 10 K/min to determine melting points ($T_m$) and

the heat of fusion ($\Delta H_f$). The heat of fusion was obtained by integration of the melting peak areas (software STAR$^e$ SW 8.10). The cocrystal yield α was calculated as

$$\alpha = \frac{\Delta H_f}{\Delta H_f^{100\%}} \quad (2)$$

With $\Delta H_f^{100\,\%}$ as heat of fusion of the cocrystals prepared by solvent evaporation (SCC 1:1).

### *Powder X-Ray Diffraction (XRD)*

The X-ray powder diffractograms were recorded at room temperature (Philips PW 1730 diffractometer, NL) using a Cu Kα radiation source with an automatic data acquisition (APD Philips v.35B). The equipment was set to a range of 2θ from 7 to 35° in the continuous mode, with a step size of 0.015° (2θ) and an acquisition time of 1 s/step. Samples were mounted on an aluminium sample holder and the amperage and voltage of the tube set to 30 mA and 40 kV, respectively.

### *Confocal Raman Microscopy (CRM) and Imaging*

Raman spectra and color-coded images were obtained using an alpha 500R Raman microscope (WiTec, Ulm, Germany) equipped with a 532 nm excitation laser, UHTS 300 spectrometer and a DV401-BV CCD camera. An area of 50 x 50 µm or 30 x 30 µm was mapped using a 40x objective (numerical aperture 1.25). Color-coded images were calculated after cosmic ray removal and baseline correction using the software WiTec Project Plus 2.10 (WiTec, Ulm, Germany).

### *Scanning Electron Microscopy (SEM)*

The surface morphology and particle shape were examined using a scanning electron microscope (DSM 940 A, Zeiss, Oberkochen, Germany). Pictures were taken using the Orion 5 frame grabber system (E.L.I. Microscopy, Charleroi, Belgium). Each sample was fixed on double-sided adhesive tape and coated with gold with a sputter coater (E5100, BioRad, München, Germany). All samples were sputtered 4 times over 60 s at 2.1 kV and 20 mA.

### *Measurement of the Specific Surface Area (BET)*

The specific surface area was determined using nitrogen gas adsorption at −196°C based on the Brunauer, Emmet and Teller (BET) method. The material was accurately weighed and analyzed with a SA 3100 Beckman Coulter system (Beckman Coulter, Krefeld, Germany). The outgas temperature was set to 25°C at an outgas time of 3 h.

### *Measurement of Dynamic Contact Angles*

The dynamic contact angles were determined using a tensiometer (K12, Krüss GmbH, Hamburg, Germany) with the modified Wilhelmy plate method [27]. Adhesive tape was cut accurately to a length of 50 mm and a height of 20 mm, attached to a Wilhelmy plate and coated with the respective powders on both sides. Superfluous material was removed by gentle air pressure. The plate was suspended from an electronic microbalance and moved with a speed of 3 mm min$^{-1}$ in and out of a test vessel containing demineralized water at 22.0°C to a maximum immersion depth of 5 mm. The contact angle $\theta$ was calculated according to

$$\cos\theta = \frac{F - F_b}{l \cdot \sigma} \quad (3)$$

Where $F$ is the measured vertical force (N), $F_b$ is the buoyancy force (N), $l$ is the wetted length (m), and $\sigma$ is the surface tension of the test liquid (Jm$^{-2}$). The buoyancy force was calculated with the laboratory desktop software 3.1 by extrapolating the graph to zero depth of immersion. The wetted length was measured with a micrometer caliper for each measurement.

## Equilibrium Solubility Studies

The solubility of IBU as a pure drug, from physical mixtures and from RESS cocrystals was determined using a 48 h shake flask method [28]. Therefore, an excess of solid (approximately 2–3 times the amount expected to achieve saturation solubility) was added to 1 ml of demineralized water in Eppendorf cups and sealed. To measure complexation between IBU and NA, known amounts of NA of increasing concentration were added to an excess of IBU [28]. The cups were placed in a thermostated water bath at 25.0°C and shaken at 60 spm for 48 h. Subsequently, the cups were centrifugated at 13,400 rpm for 20 min, the supernatant withdrawn and analyzed with HPLC (see below). The solid remnants were dried and analyzed with DSC to check for possible phase transitions.

## *In Vitro* Dissolution Studies

The *in vitro* dissolution rate was measured using a Stricker flow-through cell apparatus (Sartorius AG, Göttingen, Germany). Samples were placed into the rotating dissolution chamber together with 80 g of glass beads in 100 ml phosphate buffer pH 6.4 (Ph. Eur.) at 37.0°C. Samples of 3.5 ml were withdrawn at preset time intervals, filtered through a 0.2 µm cellulose nitrate filter and collected in test tubes. The removed sample volume was immediately replaced with fresh medium. Sample volumes were monitored and allowed a maximum deviation of±4%. The chamber volume at the

end of the test was allowed a maximum deviation of 5%. The mean dissolution time (MDT) was calculated as

$$MDT = \frac{\sum_{j=1}^{n} t_j^d \Delta M_j}{\sum_{j=1}^{n} \Delta M_j} \quad (4)$$

### Statistical Evaluation of Data

The MDT values were compared using one-way analysis of variance (ANOVA) with a significance level of 95% ($p < 0.05$) and the Scheffé test using SPSS statistics V22 (Armonk, US).

### High Pressure Liquid Chromatography (HPLC)

Concentrations of IBU and NA in aqueous solutions were measured with an HPLC system (LC 20AT, Shimadzu, Duisburg, Germany) equipped with a UV-detector (SPD-6A, Shimadzu, Duisburg, Germany) and a Nucleosil 100–5 C18 column (Macherey-Nagel, Düren, Germany). The detection wavelength was set to 230 nm. The mobile phase consisted of 60:40 (V/V) acetonitrile and 20 mM phosphoric acid pH 3.0 at a flow rate of 1.0 ml/min. The injection volume was adjusted to 20 µl.

## RESULTS

### Production of RESS IBU and RESS Coprecipitates

At a medium $CO_2$ flow rate of 3.8 kg/h, RESS IBU and RESS coprecipitates could be produced with product yields of up to 30 and 20wt%, respectively, in relation to the dissolved material. The quantitative composition of the coprecipitates was measured with HPLC and compared with the calculated molar ratio of the components in supercritical solution. Pressure loss in the extraction chamber during long extraction times caused a slight variability of the NA solubility, which explains deviations of the calculated composition of the supercritical solution from the actual molar composition of the products (Table I). Overall, it was possible to produce coprecipitates of IBU and NA in accordance with the intended molar ratio (Table I).

### Identification of Cocrystals

#### *Differential Scanning Calorimetry*

The onset temperature of melting was found to be 75.0±0.3°C for IBU and 74.5±0.7°C for RESS IBU; it was thus not affected by RESS processing (Table II). The thermal key features of cocrystals produced by solvent evaporation with a molar ratio of 1:1 (SCC 1:1) were used as reference points for RESS coprecipitates. SCC 1:1 exhibited a single sharp endotherm with an onset temperature of 90.6°C corresponding to the melting point of the cocrystal, which was in good agreement with the data reported in the literature [4, 22]. A small trace of an impurity was repeatedly detected at 64°C, which probably corresponds to a eutectic of IBU and NA (Fig. 3a). Thermograms of RESS coprecipitates with a molar ratio of 1:1 (RCC 1:1) also exhibited a single melting peak with an onset temperature of 90.2°C, while the melting points of the pure components were absent (Fig. 3a). Based on the comparison of the heat of fusion, the cocrystal yield of RCC 1:1 was found to be 0.96±0.08 (Table II), indicating that the starting material was almost completely transformed to cocrystals upon RESS precipitation. RESS coprecipitates with a molar ratio of 0.5:1 IBU:NA (RCC 0.5:1) exhibited a second broad endotherm at roughly 105°C in addition to the cocrystal melting point. This endotherm probably corresponds to NA melting in the presence of the cocrystal, since a similar endothermic event was detected in a physical mixture of cocrystals and NA (Fig. 3b). The cocrystal yield α of RCC 0.5:1 was 0.69±0.02, which indicates that IBU in these samples was almost completely transformed to cocrystals, while the superfluous amount of coformer (NA) crystallized separately. RESS coprecipitates with a molar ratio of 2:1 IBU:NA (RCC 2:1) showed two endothermic events. The first exhibited an onset temperature below those of the single components, which again probably corresponds to a eutectic of IBU and NA (65.3°C *vs.* 75.0°C for IBU and 128.6°C for NA). The second endotherm had an onset temperature below that of the cocrystal (82°C) and a broadened shape compared to the sharp cocrystal melting point. Since these samples exhibited no clear evidence of cocrystal formation, they were excluded from further analysis.

#### *Powder X-Ray Diffraction*

Diffractograms of RESS coprecipitates had reduced intensities in comparison to the unprocessed starting material and reference cocrystals. Since the thermal properties of RESS cocrystals (melting point, heat of fusion) were comparable to that of reference cocrystals, the reduced peak intensities are most probably not caused by an amorphous portion, but rather by the decreased particle size of RESS cocrystals. Diffractograms of RCC 1:1 showed characteristic peaks at 9.41° and 12.55° 2θ, which were in good agreement with the reference cocrystals produced in this study (SCC 1:1) and the literature [23, 25] (Fig. 4). The characteristic peaks of IBU (19.46° 2θ) and NA (14.87° and 27.25° 2θ) were absent in the diffraction patterns of RCC 1:1. RCC 0.5:1 exhibited the above-mentioned cocrystal peaks in addition to the NA peaks, but no IBU was detected. RCC 0.5:1 is therefore likely to be a physical mixture of the cocrystal and the coformer NA. These findings are in good

**Table I** Molar Fraction of IBU in Supercritical Solution and in RESS Products

| Sample | Molar fraction of IBU in sc solution[a] | SD* | Molar fraction of IBU in product[b] | SD* |
|---|---|---|---|---|
| RCC 1:1 | 1.01 | 0.09 | 0.94 | 0.09 |
| RCC 0.5:1 | 0.78 | 0.09 | 0.56 | 0.001 |
| RCC 2:1 | 2.12 | 0.4 | 2.05 | 0.64 |

*SD = Standard deviation

[a] Calculated by gravimetric evaluation of the remaining solid material in the extraction chamber

[b] Measured by HPLC

agreement with the DSC measurements and support that IBU was fully transformed to cocrystals upon RESS precipitation, while, if a surplus of the coformer NA was present in the supercritical solution, it was precipitated as separate crystals.

### *Confocal Raman Microscopy*

IBU and NA exhibited characteristic peaks at separate spectral regions and could therefore be well distinguished (Fig. 5a). The characteristic peaks of IBU and NA in the Raman spectra seen at 1,048 $cm^{-1}$ (NA) and 1013.5 $cm^{-1}$ (IBU) correspond to an aromatic ring deformation mode (Table III; band assignments were based on previous studies [29–31]). The characteristic C-H stretching vibrations of IBU were located in the region of 2,869 to 2,955 $cm^{-1}$, and=C-H stretching vibrations were identified for both molecules at 3,050 $cm^{-1}$ (IBU) and at 3,063 and 3,101 $cm^{-1}$ (NA). NA furthermore exhibited a weak N-H stretching mode at 3,370 $cm^{-1}$ and a $NH_2$ deformation mode at 1,620 $cm^{-1}$. For both molecules, the O-H stretching vibration was a weak band located in the region of 3,155 $cm^{-1}$ (NA) and 3,218 $cm^{-1}$ (IBU).

The Raman spectra of cocrystals exhibited characteristic bands of both components (Table III) and were equivalent for the RESS cocrystals (RCC 1:1) and cocrystals produced by slow solvent evaporation (SCC 1:1) (Fig. 5a). The peak corresponding to the C=C deformation vibration was shifted from 1,048 $cm^{-1}$ in the NA spectrum to 1,035 $cm^{-1}$ in the cocrystal spectrum. This peak was used for imaging (highlighted in Fig. 5a). Several peaks generated by structures involved in forming hydrogen bonds in the cocrystal were absent in the cocrystal spectra, including the δ $NH_2$ scissoring vibration and the v N-H stretching vibration of NA (Fig. 5b and c). Furthermore, the bonds assigned to the C=O stretching vibration at 1,680 $cm^{-1}$ (NA) and at 1,658 $cm^{-1}$ (IBU) was shifted to 1,686 $cm^{-1}$ in the cocrystal spectrum (Fig. 5b).

In Raman image scans, a sample area is scanned and a spectrum is recorded for every pixel of the image. From these data, the distribution of the material in the sample can be calculated according to the spectral information. The resulting color-coded images of the samples contain the spatially resolved chemical information of the sample. With this technique, it is possible to obtain accurate information distribution of the pure components and cocrystals throughout the RESS poducts. In image scans of physical mixtures, the single components and cocrystals could be well distinguished from each other (Fig. 6a and b). Raman imaging could thus be used as a tool to detect phase impurities in cocrystal samples, which is shown in Fig. 6c and d; where image scans of RCC 0.5:1 are depicted. In these samples, cocrystals were detected in addition to separate NA crystals while no single IBU crystals could be found (Fig. 6c and d), which supports the DSC and XRD data presented above.

**Table II** Thermal Key Features of Starting Material and RESS Products

| Sample | Molar ratio IBU:NA | T (°C) | SD* | $\Delta H_f$ (J $g^{-1}$) | SD* | α | SD* |
|---|---|---|---|---|---|---|---|
| SCC 1:1 | 1:1 | 90.6 | 0.5 | 133.2 | 2.6 | 1 | |
| RCC 1:1 | 1:1 | 90.2 | 0.4 | 127.8 | 10.4 | 0.96 | 0.08 |
| RCC 0.5:1 | 0.5:1 | 89.8 | 0.2 | 91.4 | 3.3 | 0.69 | 0.02 |
| RCC 2:1 | 2:1 | 65.2 | 0.6 | | | | |
| IBU | | 75.0 | 0.3 | 124.1 | 2.2 | | |
| RESS IBU | | 74.5 | 0.7 | 120.3 | 0.5 | | |
| NA | | 127.8 | 0.1 | 192.2 | 0.6 | | |

*SD = standard deviation

T onset temperature of melting

$\Delta H_f$ Heat of fusion at melting point

α cocrystal yield

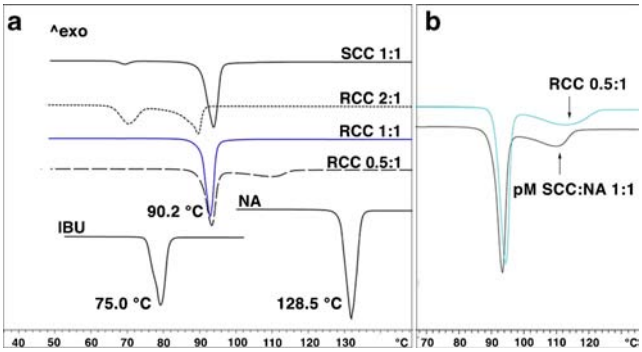


**Fig. 3** **a** DSC Thermograms of single components, RESS products and reference cocrystals; **b** Comparison of RCC 0.5:1 and a 1:1 physical mixture (pM) of cocrystal and NA.

## Characterization of the Starting Material and Cocrystals

### *Scanning Electron Microscopy (SEM)*

Scanning Electron Microscopy images revealed that IBU could be distinctly micronized by RESS processing (Fig. 7a and b). RESS IBU particles were strongly agglomerated and had heterogeneous shapes. The material seemed partly molten and fused at the edges (circled in Fig. 7b), which is possibly caused by the mantle temperature in the expansion chamber, which compensates for the cooling in the immediate expansion zone but might cause partial melting of the downstream deposited material. RESS cocrystals did not show this, which is probably due to the higher melting point and thus a higher thermal stability (90.2°C). RESS cocrystals exhibited a noticeably different morphology compared to the starting material, since they precipitated as fibers with a high aspect ratio (Fig. 7a,c,d). Judging from SEM images, the size distribution width of RESS cocrystals was comparatively large. A portion of the material formed fibers with a length that distinctly exceeded 10 μm, while another portion precipitated as considerably smaller micron particles.

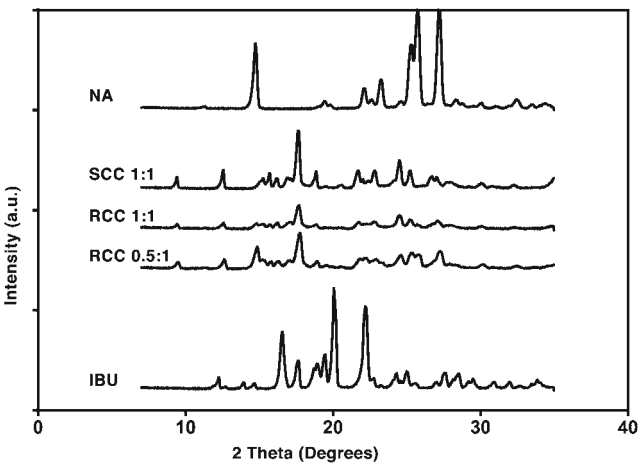


**Fig. 4** Powder X-Ray diffractograms of single components, RESS products and reference cocrystals.

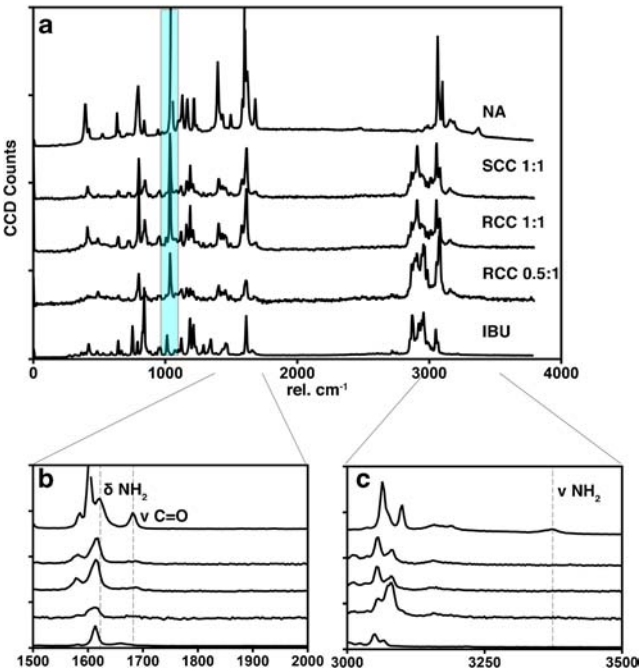


**Fig. 5** **a** Raman vibrational spectra of cocrystal samples and single components; peak positions used for imaging are highlighted. **b** Enlargement of δ $NH_2$ vibration of NA at 1,620 $cm^{-1}$ (absent in cocrystal spectra) and ν C=O vibration region (IBU: 1,658 $cm^{-1}$; NA: 1,680 $cm^{-1}$; Cocrystal (very weak): 1,686 $cm^{-1}$). **c** Enlargement of *ν* $NH_2$ vibration of NA at 3,370 $cm^{-1}$ (absent in cocrystal spectra).

### *Measurement of Specific Surface Area (BET Method)*

As a parameter correlated with particle size, we measured the specific surface area with the BET method. For RESS IBU, it was found to be roughly 4 times the surface area of unprocessed IBU (Table IV). RESS cocrystals exhibited an almost tenfold increase of the specific surface area compared to unprocessed IBU. This clearly shows the effect of RESS

**Table III** Main Vibrational Modes in the Raman Spectra of IBU, NA and Cocrystals

| Description | NA | Cocrystal | IBU |
|---|---|---|---|
| δ C=C | 1,048 | 1,035 | 1,013.5 |
| ν C-N | 1,397 | 1,403 | - |
| ν C=C | 1,600 | 1,612 | 1,613 |
| δ $NH_2$ | 1,620 | - | - |
| ν C=O | 1,680 | 1,686 | 1,658 |
| ν C-H | - | 2,866; 2,907; 2,939 | 2,869; 2,920; 2,955 |
| ν=C-H | 3,063; 3,101 | 3,050; 3,079 | 3,050 |
| ν OH | 3,155 | 3,161 | 3,218 |
| ν N-H | 3,370 | - | - |

ν: stretching; δ: deformation

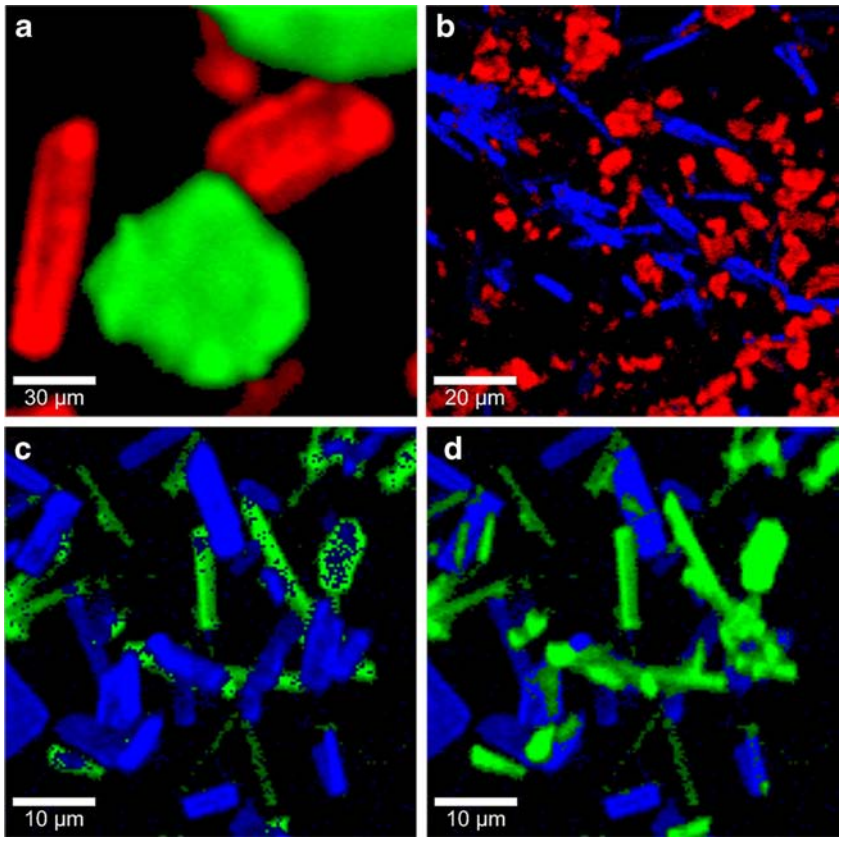


**Fig. 6** Raman image scans; color code: *red*: IBU; *blue*: Cocrystal; *green*: NA. **a**) Physical mixture of unprocessed IBU and NA; **b**) Physical mixture of RESS IBU and RCC 1:1; **c**) RCC 0.5:1; top color layer: cocrystal; **d**) RCC 0.5:1; top color layer: NA.

micronization on both the API and its cocrystal, which could already be observed in SEM images.

### *Contact Angle Measurements*

To determine the wetting properties of RESS products, the contact angle of water on the respective materials was measured. RESS IBU exhibited a distinctly increased contact angle of 91.0°±2.0° compared to unprocessed IBU (80.5°± 1.7°; Table IV). The contact angle of water on RESS cocrystals was likewise increased to 87.8°±1.1°. The same tendency was observed for cocrystals produced by slow solvent evaporation (84.4°±0.9°), although less pronounced; which shows that cocrystals independently of the production method did not exhibit a better wettability than IBU.

### *Equilibrium Solubility*

The equilibrium solubility of IBU in water at 25.0°C was found to be 0.298 mM. The equilibrium solubility of RESS IBU was slightly decreased (…), which is probably attributed to the decreased wetting ability (0.277 mM; Table V). For physical mixtures (pM) of IBU and NA, a linear increase of the equilibrium solubility of IBU was observed with increasing NA concentrations, which is in accordance with previous studies, since NA is known to form solution complexes with a variety of substances including IBU [4, 32, 33]. The solubility of IBU from RESS cocrystals was increased in the same order as observed for pM, corresponding to the concentration of NA present in the respective solutions (Table V). This shows that the increased solubility of IBU from RESS cocrystals does not depend on cocrystallization itself, but can also be achieved by the mere presence of the hydrotrope NA in the medium. DSC analysis of the solid remnants proved that they consisted of undissolved IBU with a minor trace of eutectic impurity (data not shown). NA was thus completely dissolved from the cocrystals, which indicates dissociation of the cocrystal upon dissolving [4].

### *In Vitro* Drug Dissolution

Consistent with the solubility difference between the compounds, NA dissolved much faster than IBU (Fig. 8a). Cocrystals from both production methods exhibited a distinct increase of the IBU release rate, which is in agreement with previous studies [4]. The observed increase was, however, greater for RESS cocrystals (Fig. 8b). Calculation of the mean dissolution time (MDT) and statistical analysis revealed that the MDT of IBU from RESS cocrystals was significantly decreased ($p < 0.05$) to almost the order of the faster dissolving co-former NA (Table VI). RESS micronization therefore had

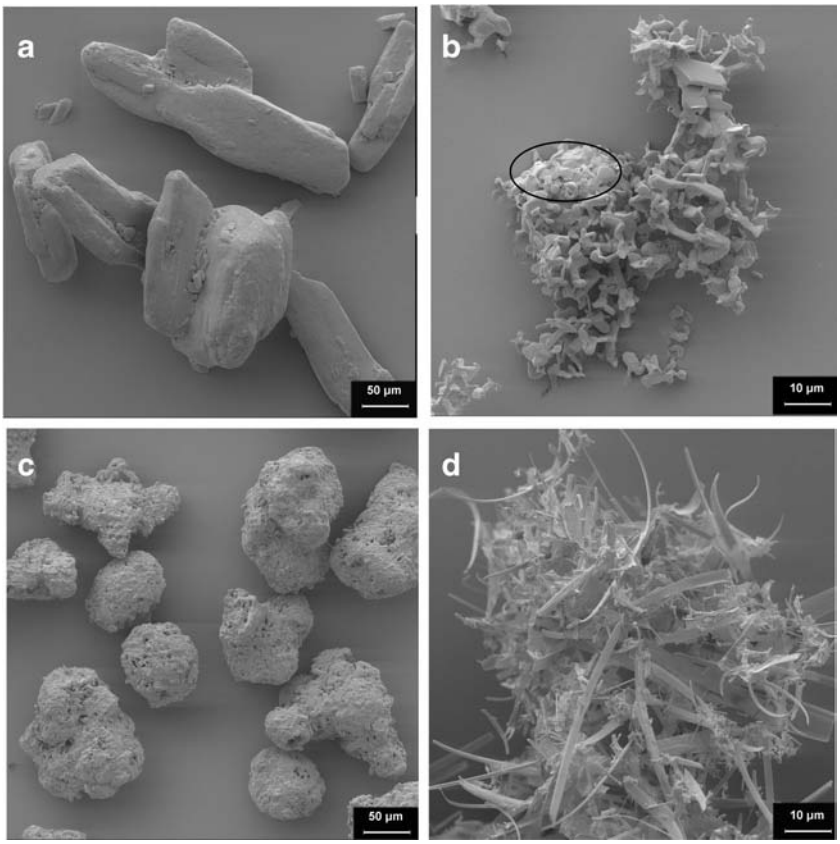


**Fig. 7** SEM images **a**) IBU; **b**) RESS IBU; **c**) NA; **d**) RCC 1:1.

an additional positive effect on the dissolution performance of IBU NA cocrystals. The release of NA from solvent cocrystals was decreased in comparison to free NA, while no effect on the MDT of NA from RESS cocrystals could be observed (Table VI).

It was interesting to observe that the MDT of NA from equimolar physical mixtures was significantly increased ($p<0.05$) compared to the MDT of the material studied alone (Table VI). SEM images of dry physical mixtures indicated an adsorption of IBU powder on the surface of NA particles, which might account for this phenomenon (data not shown). IBU from physical mixtures exhibited a similar trend towards decreased release rates, although the difference was not statistically significant (Table VI). However, no significant increase of the dissolution rate could be observed for IBU from physical mixtures, which is in accordance with previous studies [24].

**Table IV** Summary of Specific Surface Area (A) and Contact Angle (θ)

| Sample | A ($m^2$ $g^{-1}$) | SD* | θ (°) | SD* |
|---|---|---|---|---|
| IBU | 0.315 | 0.01 | 80.5 | 1.7 |
| RESS IBU | 1.38 | 0.08 | 91.0 | 2.0 |
| SCC 1:1 | 0.402 | 0.01 | 84.4 | 0.9 |
| RCC 1:1 | 2.89 | 0.22 | 87.8 | 1.1 |
| NA | 1.14 | 0.01 | 66.9 | 5.3 |

*SD = standard deviation

## DISCUSSION

In this study, we produced the 1:1 cocrystal of IBU and NA by rapid expansion of supercritical solutions (RESS) as an alternative production method for cocrystals. The RESS process offers the advantage of combining cocrystallization and micronization of the product due to the very fast precipitation conditions. DSC, XRD and CRM data showed that with the RESS technique, pure cocrystal products could be obtained. Especially Raman imaging proved to be a useful tool for the evaluation of successful cocrystal conversion and the detection of phase impurities. The key characteristics such as the melting endotherm, the X-ray diffraction pattern and Raman vibrational modes were equivalent for cocrystals produced by the RESS technique (RCC) and cocrystals prepared by slow solvent evaporation (SCC). The molecular constitution of the formed compounds was thus identical.

Cocrystal precipitation from supercritical fluids is different from precipitation from organic solvents mainly in the speed with which the products are formed and the fact that in the RESS process, no equilibria between the crystallized solid

**Table V** Equilibrium Solubility (mM) of IBU from Physical Mixtures (pM) and RESS Cocrystals In Dependence of the NA Concentration

| NA concentration (mM) | | | | | | | | |
|---|---|---|---|---|---|---|---|---|
| | 0 | SD* | 20 | SD* | 30 | SD* | 40 | SD* |
| RESS IBU | 0.277 | 0.001 | - | | - | | - | |
| Physical mixture | 0.298 | 0.049 | 0.9122 | 0.091 | 0.992 | 0.097 | 1.116 | 0.097 |
| RCC 1:1 | - | - | 0.863 | 0.145 | 0.993 | 0.043 | 1.065 | 0.062 |

*SD = standard deviation

product and the cocrystal formers in supercritical solution exist. In the RESS process, the precipitation of the solutes is irreversible, since after expansion, the fluid returns to the gaseous state, in which it has most negligible solvent power [34]. In contrast to this, for ternary systems of cocrystal formers in an organic solvent the equilibria between solid phase and the cocrystal formers in solution must be considered, since during slow evaporation of the solvent, the system may pass through several phase regions in the ternary phase diagram, which may result in precipitation of the cocrystal as well as of the pure coformer and the pure API [3]. This again is dependent on the solubility limits of the cocrystal and the respective cocrystal formers.

Successful cocrystal precipitation from supercritical solutions seems to mainly depend on the concentration of the cocrystal formers in supercritical solution. Our data indicate

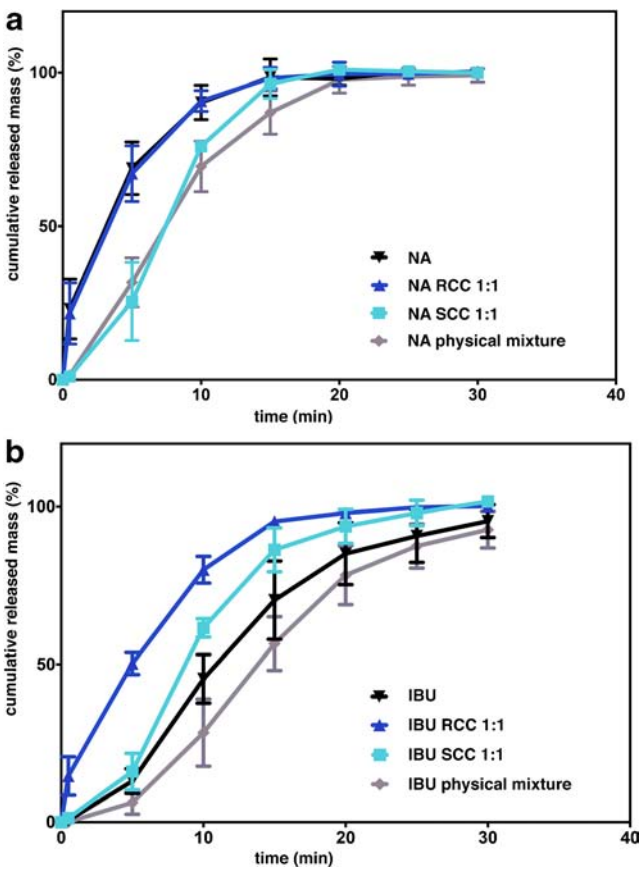


**Fig. 8** **a** Comparison of *in vitro* dissolution profiles from different formulations of **a**) NA; **b**) IBU.

that a surplus of coformer preferentially leads to the precipitation of the cocrystal plus solid coformer, while a surplus of API leads to precipitation of a mixed solid phase. It is most essential to consider the solubility limits of the cocrystal formers in $scCO_2$ at the respective dissolution conditions, since otherwise, the composition of the supercritical solution may not allow the formation of a pure cocrystal product. This issue has been taken into account in previous works as an explanation for unsuccessful cocrystallization attempts from supercritical solution, but has so far not been addressed sufficiently in an experimental manner [18, 20]. Our work now shows that it is possible to match the stoichiometry of the components in supercritical solution to produce a cocrystal product with high purity, even though the solubility of the components we used differs by an order of magnitude [21, 26]. A large difference in solubility of the components in the supercritical solvent could however theoretically prohibit successful cocrystal precipitation. As stated above, the supersaturation during expansion, which depends on the solubility of the solute, plays a fundamental role in the RESS process, since it is the driving force for nucleation and particle growth [5]. A substance with higher solubility in the respective fluid undergoing the same expansion path as a substance with lower solubility will experience a different supersaturation rate. For the two solutes, particle nucleation will thus be theoretically induced at different spatial or time coordinates regarding the expansion path [7]. Nevertheless, a simultaneous precipitation of both components is plausible, if the affinity of the coformer is sufficiently high towards the host molecule in relation to the solvent. A phase transition of the components would then coincide and dictate the nucleation and growth rate of the cocrystal [18].

The formation of solid dispersions of the additive in the host matrix causing an amorphous conversion was observed during cocrystallization experiments *via* RESS in a previous study, which was attributed by the authors to the composition of the ternary mixtures prior to expansion [18]. In the present study however, the cocrystal product we obtained *via* RESS precipitation was mainly crystalline. Amorphous conversion was observed neither for cocrystals nor for RESS IBU, which is possibly attributed to the material itself and/or the expansion conditions. Regarding stability issues associated with amorphous materials, the advantage of a highly crystalline product is evident.

A hydrotropic effect of NA increasing the aqueous solubility of IBU could be observed for both physical mixtures and

**Table VI** Mean Dissolution Time (MDT; min) of IBU and NA from Different Formulations

| | Unprocessed | SD* | SCC 1:1 | SD* | RCC 1:1 | SD* | Physical Mixture | SD* |
|---|---|---|---|---|---|---|---|---|
| IBU | 10.9[a;b] | 1.0 | 10.0[b] | 1.1 | 6.2[c] | 0.6 | 13.3[a] | 1.4 |
| NA | 4.8[a] | 0.3 | 7.7[b] | 0.6 | 4.6[a] | 0.8 | 8.1[b] | 1.2 |

*SD = standard deviation

Values with different letters a-c in a row are significantly different at $p < 0.05$ (Scheffé Test)

cocrystals. The dissolution rate of IBU was however only increased for cocrystals. The mere presence of the coformer in the dissolution medium alone does therefore not affect the dissolution speed but the components need to be presented in cocrystalline state in order to achieve the latter.

Cocrystals from both production methods exhibited an increased dissolution rate of IBU in comparison to the unprocessed material. The effect we observed was however greater for RESS cocrystals; the production method therefore had a significant impact on the dissolution rate of cocrystals. This is not attributed to a difference in wettability, since the contact angle of water was nearly the same for cocrystal samples from both production methods. RESS cocrystals exhibited a slightly increased contact angle in comparison to solvent cocrystals, which probably does not indicate an increased hydrophobicity of the cocrystal itself but rather reflects effects of different particle size and/or a higher surface roughness, since the same was observed for RESS IBU [27]. The significantly increased dissolution rate of IBU from RESS cocrystals can therefore be attributed to the larger specific surface area and thus reduced particle size of RESS cocrystals. NA from solvent cocrystals showed a decreased dissolution rate, which indicates that the entrapment of the coformer NA in a matrix of less soluble IBU molecules inhibited its release. For RESS cocrystals, this effect was not observed, which again is most probably attributed to the overall larger surface area available for dissolution. The combination of cocrystallization and micronization may therefore distinctly improve the bioavailability of drug candidates with dissolution-limited bioavailability und thus, ultimately, decrease dosages.

## CONCLUSIONS

In this study we successfully produced the 1:1 cocrystal of IBU and NA with the RESS process. Our results show that with RESS, a crystalline micronized cocrystal product with the correct stoichiometric composition can be produced in a single step operation without the need of further processing such as drying or size reduction. In comparison to established size reduction techniques, RESS offers unique qualities such as mild processing conditions and a very low environmental impact due to the absence of organic solvents, which becomes more and more important in today's environment that is increasingly focused on sustainability. This is also true for the formation of cocrystals, which are often produced by recrystallization from organic solvents. Employing RESS provides a product free of toxic contamination. The rather low throughput rates of RESS can be overcome by continuously running processes with closed loop technique for recycling of the fluid and the use of nozzle arrays, which can open the way for this technique into production.

Given sufficient solubility of the cocrystal formers in the respective supercritical fluid, cocrystal formation *via* RESS thus might present a superior alternative to established production methods.

## ACKNOWLEDGMENTS AND DISCLOSURES

A part of this work has been presented as a poster at the AAPS Annual Meeting in San Antonio, US, Nov. 10–14, 2013 and at the 9th PBP world meeting in Lisbon, Portugal, March 31—April 3.

## REFERENCES

1. Elder DP, Holm R, Diego HL. Use of pharmaceutical salts and cocrystals to address the issue of poor solubility. Int J Pharm. 2013;453(1):88–100.
2. U.S. Food and Drug Administration 2013. U.S. Department of Health and Human Services, Food and Drug Administration, Center for Drug Evaluation and Research. Guidance for Industry: Regulatory Classification of Pharmaceutical Cocrystals.
3. Ainouz A, Authelin J-R, Billot P, Lieberman H. Modeling and prediction of cocrystal phase diagrams. Int J Pharm. 2009;374(1–2):82–9.
4. Chow SF, Chen M, Shi L, Chow AHL, Sun CC. Simultaneously improving the mechanical properties, dissolution performance, and hygroscopicity of ibuprofen and flurbiprofen by cocrystallization with nicotinamide. Pharm Res. 2012;29(7):1854–65.
5. Debenedetti PG, Tom JW, Kwauk X, Yeo SD. Rapid expansion of supercritical solutions (RESS): fundamentals and applications. Fluid Phase Equilib. 1993;82:311–21.
6. Hirunsit P, Huang Z, Srinophakun T, Charoenchaitrakool M, Kawi S. Particle formation of ibuprofen-supercritical CO2 system from

rapid expansion of supercritical solutions (RESS): a mathematical model. Powder Technol. 2005;154(2–3):83–94.
7. Türk M. Formation of small organic particles by RESS: experimental and theoretical investigations. J Supercrit Fluids. 1999;15(1):79–89.
8. Türk M, Hils P, Helfgen B, Schaber K, Martin HJ, Wahl MA. Micronization of pharmaceutical substances by the Rapid Expansion of Supercritical Solutions (RESS): a promising method to improve bioavailability of poorly soluble pharmaceutical agents. J Supercrit Fluids. 2002;22(1):75–84.
9. Ginty PJ, Whitaker MJ, Shakesheff KM, Howdle SM. Drug delivery goes supercritical. Mater Today. 2005;8(8):42–8.
10. Vemavarapu C, Mollan MJ, Lodaya M, Needham TE. Design and process aspects of laboratory scale SCF particle formation systems. Int J Pharm. 2005;292(1):1–16.
11. Constable DJC, Jimenez-Gonzalez C, Henderson RK. Perspective on solvent use in the pharmaceutical industry. Org Process Res Dev. 2006;11(1):133–7.
12. Pasquali I, Bettini R, Giordano F. Solid-state chemistry and particle engineering with supercritical fluids in pharmaceutics. Eur J Pharm Sci. 2006;27(4):299–310.
13. Pasquali I, Bettini R. Are pharmaceutics really going supercritical? Int J Pharm. 2008;364(2):176–87.
14. Jung J, Perrut M. Particle design using supercritical fluids: literature and patent survey. J Supercrit Fluids. 2001;20(3):179–219.
15. Wahl MA. Supercritical fluid technology. In: Parikh DM, editor. Handbook of pharmaceutical granulation technology. New York: Informa Healthcare; 2009. p. 126–37.
16. Hezave AZ, Esmaeilzadeh F. Micronization of drug particles *via* RESS process. J Supercrit Fluids. 2010;52(1):84–98.
17. Kayrak D, Akman U, Hortaçsu Ö. Micronization of ibuprofen by RESS. J Supercrit Fluids. 2003;26(1):17–31.
18. Vemavarapu C, Mollan MJ, Needham TE. Coprecipitation of pharmaceutical actives and their structurally related additives by the RESS process. Powder Technol. 2009;189(3):444–53.
19. Johannsen M, Brunner G. Measurements of solubilities of xanthines in supercritical carbon dioxide + methanol. J Chem Eng Data. 1995;40(2):431–4.
20. Padrela L, Rodrigues MA, Velaga SP, Matos HA, de Azevedo EG. Formation of indomethacin-saccharin cocrystals using supercritical fluid technology. Eur J Pharm Sci. 2009;38(1):9–17.
21. Charoenchaitrakool M, Dehghani F, Foster NR, Chan HK. Micronization by rapid expansion of supercritical solutions to enhance the dissolution rates of poorly water-soluble pharmaceuticals. Ind Eng Chem Res. 2000;39(12):4794–802.
22. Oberoi LM, Alexander KS, Riga AT. Study of interaction between ibuprofen and nicotinamide using differential scanning calorimetry, spectroscopy, and microscopy and formulation of a fast-acting and possibly better ibuprofen suspension for osteoarthritis patients. J Pharm Sci. 2004;94(1):93–101.
23. Berry DJ, Seaton CC, Clegg W, Harrington RW, Coles SJ, Horton PN, *et al.* Applying hot-stage microscopy to co-crystal screening: a study of nicotinamide with seven active pharmaceutical ingredients. Cryst Growth Des. 2008;8(5):1697–712.
24. Dhumal RS, Kelly AL, York P, Coates PD, Paradkar A. Cocrystalization and simultaneous agglomeration using hot melt extrusion. Pharm Res. 2010;27(12):2725–33.
25. Kelly AL, Gough T, Dhumal RS, Halsey SA, Paradkar A. Monitoring ibuprofen-nicotinamide cocrystal formation during solvent free continuous cocrystallization (SFCC) using near infrared spectroscopy as a PAT tool. Int J Pharm. 2012;426(1–2):15–20.
26. Kotnik P, Škerget M, Knez Ž. Solubility of nicotinic acid and nicotinamide in carbon dioxide at T=(313.15 to 373.15) K and p=(5 to 30) MPa: experimental data and correlation. J Chem Eng Data. 2011;56(2):338–43.
27. Sheridan PL, Buckton G, Storey DE. The extent of errors associated with contact angles II. factors affecting data obtained using a Wilhelmy plate technique for powders. Int J Pharm. 1994;109(2):155–71.
28. Grossjohann C, Eccles KS, Maguire AR, Lawrence SE, Tajber L, Corrigan OI, *et al.* Characterisation, solubility and intrinsic dissolution behaviour of benzamide: dibenzyl sulfoxide cocrystal. Int J Pharm. 2012;422(1–2):24–32.
29. Akalin E, Akyuz S. Vibrational analysis of free and hydrogen bonded complexes of nicotinamide and picolinamide. Vib Spectrosc. 2006;42(2):333–40.
30. Rossi B, Verrocchio P, Viliani G, Mancini I, Guella G, Rigo E, *et al.* Vibrational properties of ibuprofen–cyclodextrin inclusion complexes investigated by Raman scattering and numerical simulation. J Raman Spectrosc. 2009;40(4):453–8.
31. Jubert A, Legarto ML, Massa NE, Tévez LL, Okulik NB. Vibrational and theoretical studies of non-steroidal anti-inflammatory drugs Ibuprofen [2-(4-isobutylphenyl)propionic acid]; Naproxen [6-methoxy-α±−methyl-2-naphthalene acetic acid] and Tolmetin acids [1-methyl-5-(4-methylbenzoyl)-1H-pyrrole-2-acetic acid]. J Mol Struct. 2006;783(1–3):34–51.
32. Truelove J, Bawarshi-Nassar R, Chen NR, Hussain A. Solubility enhancement of some developmental anti-cancer nucleoside analogs by complexation with nicotinamide. Int J Pharm. 1984;19(1):17–25.
33. Sanghvi R, Evans D, Yalkowsky SH. Stacking complexation by nicotinamide: a useful way of enhancing drug solubility. Int J Pharm. 2007;336(1):35–41.
34. Matson DW, Fulton JL, Petersen RC, Smith RD. Rapid expansion of supercritical fluid solutions: solute formation of powders, thin films, and fibers. Ind Eng Chem Res. 1987;26(11):2298–306.